Analysis of Composites with Infrared Thermography

*Carosena Meola,**[1] *Giovanni Maria Carlomagno,*[1] *Antonino Squillace,*[2] *Umberto Prisco,*[2] *Renata Erica Morace*[2]

[1]Department of Energetics, Thermofluidynamics and Environmental Control (DETEC), University of Naples Federico II, P.le Tecchio, 80, 80125 Naples, Italy
Fax: (39) 0817683389; E-mail: carmeola@unina.it
[2]Department of Materials and Production Engineering (DIMP), University of Naples Federico II, P.le Tecchio, 80, 80125 Naples, Italy

Summary: The aim of this study was a non-destructive evaluation of composites through their behaviour under thermal stimulation. Such behaviour was monitored by infrared thermography. Several specimens were fabricated involving: glass/epoxy with inclusion of foreign materials; carbon/epoxy with backdrilled holes; carbon/epoxy with impact damage; Glare® failed in bearing way. The obtained results prove that infrared thermography is capable of detecting the materials inhomogeneities and/or damage listed above. In particular, lock-in thermography is capable of supplying useful information about: the distribution of the adhesive thickness in composite structures; the distribution of the paint thickness; the behaviour under load of aluminium layers and glass fibres in Glare®.

Keywords: fibre reinforced composites; Glare®; infrared thermography; non-destructive evaluation

Introduction

Infrared thermography (IRT) is a non-contact, non-intrusive technique of surface temperature mapping, which can be exploited in a vast variety of industrial as well as research fields. IRT detects the energy radiated from objects in the infrared band of the electromagnetic spectrum and converts it into a visible image; each energy level may be represented by a colour, or a gray level. The temperature represents a critical parameter in many steps of manufacturing processes. Cooling efficiency plays a key role in material *shaping* (extrusion, moulding) and in material *removal* (milling finish, drilling). The temperature is also an important parameter for curing of polymers in autoclave. However, the surface temperature measurement can be exploited for non-destructive evaluation of materials and structures. Thus, infrared thermography can be used to monitor the entire life of a component through three main passages: assessment of manufacturing processes, non-destructive evaluation of final products and in service maintenance.

 DOI: 10.1002/masy.200551025

In particular, non-destructive evaluation can supply information for material acceptance/rejection and machine performance assessment if performed at every manufacturing step. The analysis of subsurface features in solid objects by infrared thermography generally requires heat energy to be transferred to the object in the active mode and monitoring the material response to such stimulation. Basically, two techniques can be used: pulse thermography (PT), lock-in thermography (LT).

In pulse thermography the infrared camera monitors the manufact surface temperature variation during the transient heating (cooling) phase. Data are represented as thermal images where each colour, or grey level, is associated to a temperature value. Depth, size and thermal resistance of defects can be estimated by processing the signal. Cielo et al. [1] described several PT applications to the evaluation of industrial materials and related the thermal propagation time to the depth and thickness of defects. Vavilov [2] highlighted the image processing techniques which relate the temperature variation to the defect properties (thermal resistance, size, depth etc.). Giorleo and Meola [3] considered defective glass/epoxy laminates and proposed a method to measure depth and size of defects. In particular, they analysed the time-sequence images in terms of temperature differences, ΔT, between sound and damaged zones and estimated the minimum ΔT value to be considered as defect contour. The PT technique is affected by the local variation of the emissivity coefficient and non-uniform heating that can mask the defect visibility.

A technique which allows overcoming these two drawbacks is the lock-in thermography. Such technique was first described by Carlomagno and Berardi [4] and later further investigated by other researchers [5-7]. The lock-in technique uses thermal waves instead of pulses. The modulated heat transfer can be described in terms of a heavily damped wave where both real and imaginary parts of the complex wave number are expressed in terms of the inverse of the thermal diffusion length μ, which is given by the relationship:

$$\mu = \sqrt{\frac{\alpha}{\pi f}} \tag{1}$$

where α is the material thermal diffusivity and f is the thermal wave frequency. Data can be represented as amplitude, or phase, images. The depth range, for the amplitude image, is given by μ while the maximum depth, p, which can be inspected, for the phase image corresponds to:

$$p = 1.8\,\mu \tag{2}$$

LT has been used to acquire information about the fibre orientation in composites [8], to visualize delaminations of veneered wood [9], to measure thickness, and/or density, and/or porosity of ceramic coatings [10]. Over the last few years lock-in thermography was applied for non-destructive evaluation of several different materials, bonded structures and joints obtained with both adhesive bonding and welding [11-15].

Another technique which combines advantages (without sharing drawbacks) of both PT and LT is the pulse phase thermography (PPT) [16]. In PPT the specimen is pulse heated as in PT and the mix of frequencies of the thermal waves launched into the specimen is unscrambled by performing the Fourier transform of the temperature evolution over the field of view. Data can be presented as amplitude, or phase, images as in LT. A comparison between the different techniques was performed by Carlomagno and Meola [17]. However, there are other techniques such as time-resolved-infrared (TRIR), vibrothermography, etc. which are variations of PT and LT because they include a different heating method, or a different processing algorithm. For more details refer to the review article by Meola and Carlomagno [18].

In this study PT and LT techniques were used for non-destructive evaluation of glass and carbon reinforced resin epoxy composites and hybrid composites (Glare®).

Materials and methods

Description of specimens

The specimens herein analysed were either home made (glass/epoxy, carbon/epoxy) with inclusion of foreign materials to simulate delaminations and/or inhomogeneities, or were pieces cut from laminates (carbon/epoxy, Glare®), which were supplied by Alenia Aerospazio (Italy). Such specimens can be divided into three groups: glass/epoxy, carbon/epoxy and hybrid composites.

Glass reinforced resin epoxy composites

Several specimens with inserts of both circular and rectangular shape were considered. Each specimen was obtained by assembling two, or three prepregs. First, prepregs were fabricated by overlaying a certain number (depending on the desired thickness, s) of resin epoxy preimpregnated glass fabric $(0,90)_f$ layers and cured in a press at ambient temperature. Then, some prepregs were perforated for inserts housing and filled with aluminium, cork, or Teflon. At the end the prepreg with inserts, after epoxy adhesive was

applied to each side, was positioned between two sound prepregs and cured in a press at ambient temperature. A sketch of a specimen with circular inserts is shown in Figure 1.

To permit analysis of low-depth defects, two prepregs, one sound and the other with inserts, were also assembled. In this case, the two prepregs were placed in contact with epoxy adhesive and, to avoid defects protrusion, a layer of epoxy adhesive, of thickness s = 0.125 mm, was applied to the outside of the prepreg with inserts. The size of each specimen was 150×150 mm^2 with a thickness of about 5 mm. Circular defects had diameter d equal to 2, 3, 4, 6 and 8 mm; rectangular defects instead were 2×14, 3×11, 3×18, 3×21 and 3×24 mm^2. The prepreg thickness was varied to have defects positioned at different depths p from 0.125 up to 4 mm. It has to be noted that, apart from the specimens with defects at p = 2 mm, the same specimen contains defects at two depths (i.e. 0.125 and 4 mm, 1 and 3 mm) by viewing it from one side, or the opposite one. The specimens were named with the following notations: GFRP-C# and GFRP-R# where C and R indicate respectively circular and rectangular defects, the symbol # represents the material of which inserts were made and is replaced with A (aluminium), C (cork) and T (Teflon).

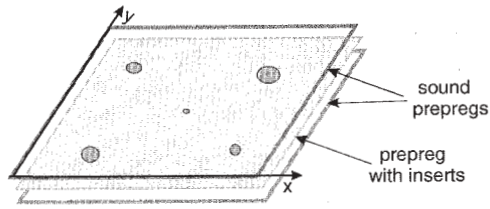

Figure 1. Sketch of glass/epoxy specimens with circular inserts (GFRP-C).

Carbon reinforced resin epoxy composites

Three specimens named CFRP-1, CFRP-2 and CFRP-3 were prepared.

The specimen CFRP-1 was obtained by overlaying several epoxy adhesive preimpregnated carbon fabric $(0,90)_f$ layers and cured in a press at ambient temperature. This specimen was 150 mm long, 135 mm wide and 8 mm thick. Holes of diameters 4, 6 and 8 mm were drilled on the backside at different depths; the holes position is depicted in Figure 2 with indication of diameter, d, and depth, p, in millimeters (p indicates the sound undrilled material thickness over each hole).

The specimen CFRP-2 is a piece of a $(0,90)_f$ laminate 3 mm thick produced by Alenia

Aerospazio (Italy). Such specimen was impacted at low load and, on the impacted side no damage was visible to naked eyes.

The specimen CFRP-3 is a piece of a $(0,90)_f$ laminate 2 mm thick produced by Alenia Aerospazio (Italy). Such specimen was coated with the green paint commonly used for the industrial production.

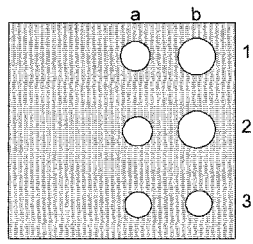

hole	d [mm]	p [mm]
a1	6	3
a2	6	5
a3	4	5
b1	8	2
b2	8	4
b3	4	6

Figure 2. Sketch of CFRP-1 specimen with indication of backdrilled holes diameter, *d*, and depth, *p*, (sound material thickness over holes).

Hybrid composites

An innovative Glare® Fiber Reinforced Metal Laminate (FRML) produced by Alenia Aerospazio (Italy) was considered; it included thin aluminium Al 7075 T-7351 layers combined with R glass fiber/epoxy layers as sketched in Figure 3a. Several pieces 20 mm wide and 50 mm long were cut from a large laminate; a hole of diameter D = 8 mm was drilled in each specimen at a position (Figure 3b) to have a width (W) to diameter ratio W/D = 2.5 and hole-to-edge distance (E) to diameter ratio E/D = 1.6.

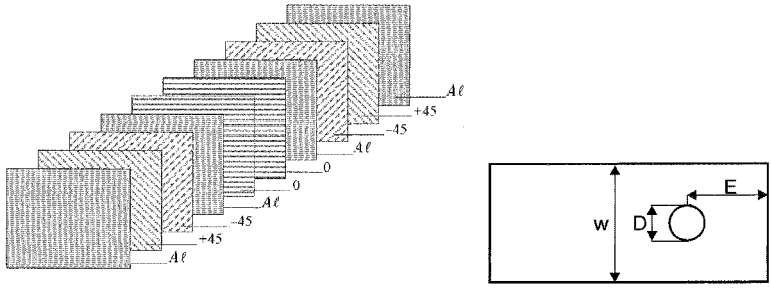

a) staking sequence b) hole position

Figure 3. Glare® specimens.

Test procedure

The experimental set up included the specimen, a heat source (quartz lamp of 1 kW) and the infrared camera Agema Thermovision 900LW [12]. The lamp was positioned at about 1 m from the specimen surface while the position of the infrared camera depended on the employed lens and on the desired field of view. Tests were performed with both PT and LT techniques.

Pulse thermography

Analysis with PT can be performed in two different ways: transmission and reflection. In the transmission mode, the infrared camera views the rear face, i.e. opposite to the heating/cooling source. In practical applications the object rear side is generally not accessible; thus the reflection mode must be used for which both infrared camera and stimulation source are located on the same side. In this study both modes were used.

The specimens with Teflon rectangular inserts (GFRP-RT) were tested in transmission mode and sequences of images at time intervals t = 2 s were acquired during the heating phase. The specimens with cork diskettes (GFRP-CC) were tested in reflection mode with images acquired during the cooling phase.

The sequences of images were later analysed to acquire information about the time-temperature variations. It is known that heat flows by conduction through the specimen thickness and needs a certain time (depending on the material thermal properties) to reach steady-state conditions. The presence of a flaw in the subsurface affects the heat flow depending on the relative thermal diffusivity $\alpha_r = \alpha_s - \alpha_d$ between the thermal diffusivity of the sound material α_s and that of the defect α_d. More specifically, if $\alpha_s > \alpha_d$ the defect opposes the flow and causes delay in the temperature rise (i.e. the defect appears as cold zone). On the contrary, if $\alpha_s < \alpha_d$ the defect favours local warming (i.e. the defect appears as hot zone).

An important parameter is the thermal contrast C_T:

$$C_T = \frac{\Delta T_d}{T_s} = \frac{T_s - T_d}{T_s} \tag{3}$$

where T_s is the temperature of the sound material and T_d is the temperature over the defect. Generally, the contrast is good for subsurface defects and worsens as the depth increases.

Lock-in thermography

The wave frequency for the Agema Thermovision 900 coupled with the lock-in option can be varied from 3.75 Hz (267 ms) down to 0.0037 Hz (273 s) in 15 intervals. The lamp was previously calibrated, for each of the employed wave frequency, to ensure that the temperature waveform was really sinusoidal. Generally, tests started at a quite high wave frequency at which, depending on the material diffusivity, only surface (or low depth) defects were visible; and later on, to visualize deeper layers, the frequency was decreased until the entire thickness had been inspected, or the minimum selectable value ($f = 0.0037$ Hz) had been reached. In this study data were presented as phase images; colour variations indicate phase angle variations. The images were stored for further analysis.

Results and discussions

Glass/epoxy specimens

Two thermal images of the specimen GFRP-RT are shown in Figure 4. The first image (Figure 4a) was taken, after $t = 14$ s to lamp exposure, by viewing the specimen side with defects located at $p = 0.125$ mm. The second image (Figure 4b) was instead taken, after $t = 26$ s to lamp exposure, by viewing the rear side of the specimen with defects located at $p = 4$ mm. As can be seen defects at p = 0.125 mm (Figure 4a) are all clearly visible and they appear darker with respect to the sound material; the sound material is characterized by an almost uniform temperature distribution. As the depth increases the contrast worsens and defects at p = 4 mm (Figure 4b) appear defocused; the temperature distribution over the sound material is not uniform. This behaviour can be ascribed to two main factors: thermal spreading within the material and natural convection. It has to be noted that deeper defects became visible later (26 s) with respect to the surface ones (14 s); lengthening the heat exposure favours both factors. In addition, thermal spreading inside the material increases with the thickness.

The thermal images were analysed in terms of temperature distribution along lines through the defects center. The time-temperature distribution along the lines A and C, parallel to the x axis (Figure 4b) for each image of the sequence is shown in Figure 5. In particular, the temperature distribution along the line A crossing the two defects 2×14 and 3×21 mm^2 is shown in Figure 5a, while the temperature distribution along the line C crossing the two defects 3×11 and 3×18 mm^2 is shown in Figure 5b.

Note that the specimen surface temperature, initially ($t = 0$ s) equal to the ambient

temperature, after exposure to heating begins to increase and shows local minima over defects. Teflon has thermal diffusivity lower than the sound glass/epoxy and causes heating delay; thus, defects are characterized by a lower temperature value. The temperature difference ΔT_d (Eq.3) for the first few seconds is of the same order of the signal noise and no measurement is reliable; later ΔT_d increases and for t = 30 s all the four defects are clearly distinguishable.

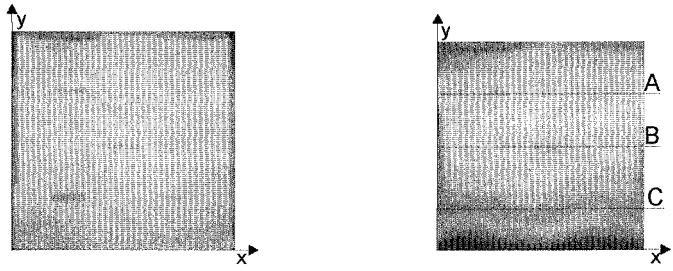

a) p = 0.125 mm, t = 14 s b) p = 4 mm, t = 26 s

Figure 4. Thermal images of GFRP-RT specimens acquired during transient heating.

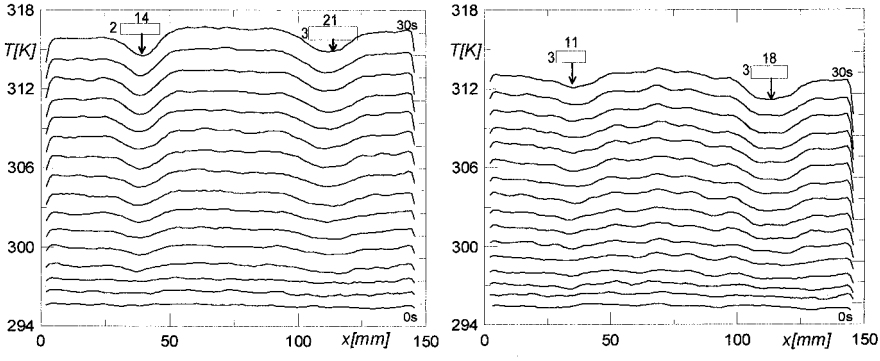

a) line A b) line C

Figure 5. Temperature profiles along lines A and C of Figure 4b.

After 30 s heating, the temperature values T along the line C, crossing the defects 3×11 and 3×18 mm^2, and along the line B, crossing the defect 3×24 mm^2, were normalized with respect to the temperature in a sound zone T_s. Profiles of $T_r = T/T_s$ are shown in Figure

6. As can be seen each defect produces a V shaped discontinuity in the T_r distribution with minimum in the defect centre and of magnitude proportional to the defect size. Such V shape could be affected by non-uniform heating of the specimen surface. The defect width can be evaluated by following the criterion of the middle height experimentally found by Giorleo and Meola [3, 11] from considerations of heat transfer mechanisms and noise signal in glass/epoxy laminates.

The C_T values for rectangular defects 3×21 mm^2 are plotted against the depth in Figure 7; C_T decreases with the power law $C_T = 0.01p^{-0.86}$ with $R^2 = 0.9$.

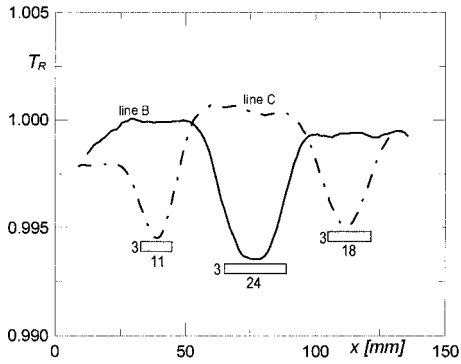

Figure 6. T_r distribution along lines C (defects 3×11, 3×18 mm^2) and B (defect 3×24 mm^2) of Figure 4b for the GFRP-RT specimen.

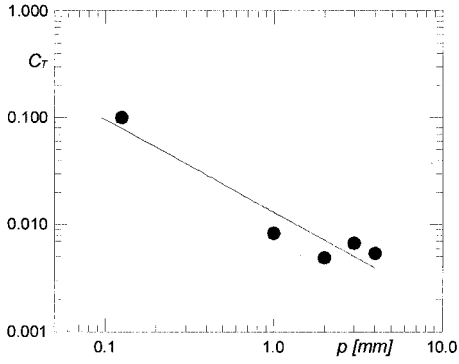

Figure 7. Distribution of C_T with depth for GFRP-RT specimens.

A thermal image, taken during transient cooling, of the specimen GFRP-CC with cork defects 2 mm deep is shown in Figure 8. Defects appear as hot spots because cork, which is a porous medium filled with air, acts as local thermal insulation opposing the heat flow. A phase image, taken at $f = 0.047$ Hz, of the specimen GFRP-CC with cork defects 2 mm deep is shown in Figure 9. Such image is characterized by a light background with two darker vertical-oblique bands. Darker areas indicate either the presence of defects, or a thicker layer of adhesive; defects are not all clearly distinguishable. One could infer that LT is not capable of detecting the presence of cork diskettes inside glass/epoxy. Indeed, lock-in thermography is capable of discriminating between resin epoxy and glass-fibers materials [19] and also between materials of close thermal properties [20]. A probable explanation is that cork, which possesses the natural tendency to absorb liquids, got impregnated with epoxy adhesive during prepregs assembling; this masked defects visibility.

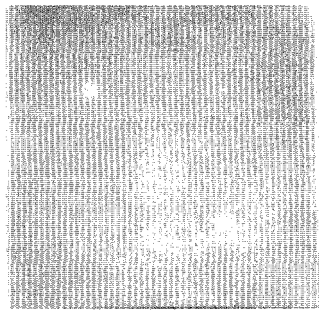

Figure 8. Thermal image acquired during transient cooling of the GFRP-CC specimen for $p = 1$ mm.

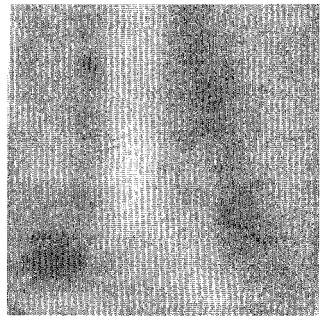

Figure 9. Phase image taken at $f = 0.047$ Hz of the GFRP-CC specimen for $p = 2$ mm.

Carbon/epoxy specimens

A phase image of the specimen CFRP-1 taken at f = 0.0072 Hz is shown in Figure 10. Note that images were acquired by viewing the side opposite to that of drilling. As can be seen the image shows darker zones over an almost uniform light background. More specifically, the three dark spots encircled on the right side correspond to the holes a1, b1 and b2 (Figure 2), which have large diameter and low depth. However, there are dimly signs of the other holes over the two dark vertical bands; a better defects visibility would be possible by lowering the heating frequency.

An important observation is the presence of darker and lighter spots on the left hand side where the material should be sound because no defects (backdrilled holes) were artificially created there. Such spots most probably are due to impact damage caused when placing the specimen into the press during fabrication; we think that breakage of carbon fibers occurred with local formation of air bubbles.

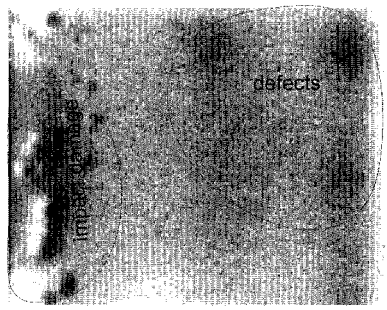

Figure 10. Phase image taken at f = 0.0072 Hz of the CFRP-1 specimen.

Two phase images of the specimen CFRP-2 are shown in Figure 11. For f = 0.47 Hz (Figure 11a) only weak signs of impact damage are visible; at this frequency, the phase angle distribution refers to the material conditions at depth of about 1 mm. As the frequency was reduced to 0.12 Hz (Figure 11b), for which the wave reached the layer about 2 mm deep, the characteristic lobed appearance of the impact damage appeared.

Two phase images of the specimen CFRP-3 are shown in Figure 12. The first image (Figure 12a), which was taken at f = 0.47 Hz is characterized by a quite uniform colour, which stands for uniform phase angle distribution. By decreasing the heating frequency to 0.23 Hz (Figure 12b) the phase angle distribution shows local variations. In particular,

dark zones indicate a thicker paint layer, while the light colour indicates that locally the wave has reached the carbon/epoxy under the paint. This demonstrates the capability of LT to provide indications about the distribution of the paint layer thickness.

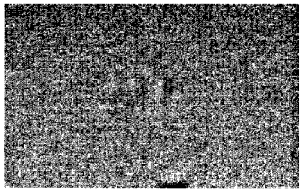

a) f = 0.47 Hz

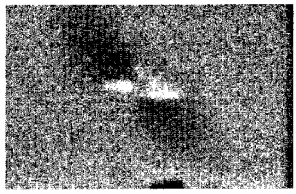

b) f = 0.12 Hz

Figure 11. Phase images of the impacted specimen CFRP-2.

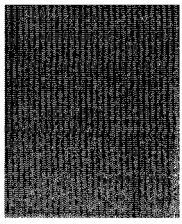

a) f = 0.47 Hz

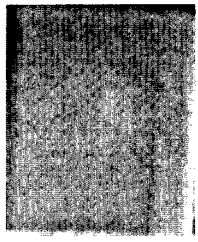

b) f = 0.23 Hz

Figure 12. Phase images of the CFRP-3 specimen.

Glare® specimens

Glare® specimens were non-destructively evaluated with lock-in thermography before and after bearing failure. Specimens were tested in pin bearing way without lateral restraints [21]. The phase images taken at f = 0.058 Hz are shown in Figure 13. The first image (Figure 13a) of the unloaded specimen indicates good material conditions without any significant delaminations induced by drilling. On the contrary, the image of the specimen, failed in bearing way (Figure 13b), is characterized by a lighter arc on the right hand side, which indicates bending of the aluminium layers and delamination and displacement of glass fibers. It is worth noting that LT, by varying the heating frequency, provides information about the behaviour under load of the different layers of aluminium, glass fibers and adhesive [15].

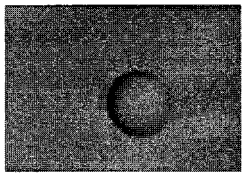

a) unloaded

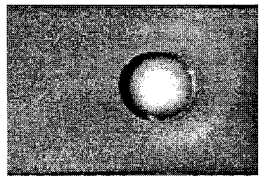

b) after bearing failure

Figure 13. Phase images of Glare® specimens taken at $f = 0.058$ Hz.

Conclusions

From data shown in this paper and also those reported in previous studies [11-15, 17-20], it is possible to infer that:

- Pulse thermography is mainly capable of detecting inclusions of foreign materials, formation of air bubbles, impact damage, disbondings and delaminations in composite structures.
- Besides the above defects, lock-in thermography is also capable of supplying information about the adhesive thickness, the paint thickness, the fibres stacking sequence and the influence of substrates surface treatments on adhesion.

The main advantages of infrared thermography are: non-contact, non-intrusive, two-dimensionality, remote imaging of large areas. Notwithstanding this, infrared thermography is still not completely exploited since it is not adequately enclosed in industrial testing perhaps because of lack of adequate knowledge and since, at first sight, it seems too expensive and difficult to use.

Acknowledgments

The authors wish to thank the staff of Alenia Aerospazio (Italy) for materials

[1] P. Cielo, X. Maldague, A.A. Déom, R. Lewak, *Mat. Eval.* **1987,** *45*, 452.
[2] V. Vavilov, in: Proc. *Qirt 92,* D. Balageas, G. Busse and G.M. Carlomagno Eds. EETI editions Paris, 1992, p. 179.
[3] G. Giorleo, C. Meola, *ASM Int. J. Mater. Eng. Perform.*, **1998,** *7*, 367.
[4] G.M. Carlomagno, P.G. Berardi, in: Proc. *3rd Infrared Information Exchange*, C. Warren Ed., St. Louis/USA, 1976, p. 33.
[5] J.-L. Beaudoin, E. Merienne, R. Danjoux, M. Egee, in: Proc. *SPIE 590*, 1985, p. 287.
[6] P.K. Kuo, Z.J. Feng, T. Ahmed, L.D. Favro, R.L. Thomas, J. Hartikainen, in: Proc. *Photoacoustic and Photothermal Phenomena,* P. Hess, J. Pelzl Eds., Springer-Verlag, Heidelberg., 1987, p. 415.
[7] G. Busse, D. Wu, W. Karpen, *J. Appl. Phys.* **1992,** *71*, 3962.
[8] W. Karpen, D. Wu, R. Steegmuller, G. Busse, in: Proc. *Qirt 94,* D. Balageas, G. Busse and G.M. Carlomagno Eds., 1994, p. 281.
[9] D. Wu, in: Proc. *Qirt 94*, D. Balageas, G. Busse and G.M. Carlomagno Eds., 1994, p. 298.
[10] J. Rantala, D. Wu, G. Busse, *Res. Nondest. Eval.*, **1996,** *7,* 215.
[11] G. Giorleo, C. Meola, *NDT&E International,* **2002,** *35*, 287.
[12] C. Meola, G. Giorleo, L. Nele, A. Squillace, G.M. Carlomagno, *Nondest. Test. and Eval.,* **2002,** *18,* 83.
[13] C. Meola, G.M. Carlomagno, A. Squillace, G. Giorleo, *Meas. Sci. Techol.*, **2002,** *13,* 1583.
[14] C. Meola, G.M. Carlomagno, L. Giorleo *J. Adhesion Sci. Technol.*, **2003,** *17,* 1207.
[15] C. Meola, A. Squillace, G. Giorleo, L. Nele, *J. Comp. Mat.*, **2003,** *37*, 1543.
[16] X. Maldague, S. Marinetti, *J. Appl. Phys.*, **1996,** *79*, 2694.
[17] G.M. Carlomagno, C. Meola, *NDT&E Int.*, **2002,** *35*, 559.
[18] C. Meola, G.M. Carlomagno *Meas. Sci. Techol.*, (review article) **2004,** *15*, R27.
[19] C. Meola, G.M. Carlomagno, G. Giorleo, *J. Adhesion Sci. Technol.*, **2004,** *18*, 617.
[20] C. Meola, G.M. Carlomagno, L. Giorleo, *J. Mat. Proc. Technol.* **2004**, *155-156C*, 1132.
[21] G. Caprino, G. Giorleo, L. Nele, A. Squillace, *Comp. A: Appl. Sci. Man.*, **2002,** *33,* 779.